AAC
Journals.ASM.org

Targeted Intracellular Delivery of Antituberculosis Drugs to *Mycobacterium tuberculosis*-Infected Macrophages via Functionalized Mesoporous Silica Nanoparticles

Daniel L. Clemens,[a] Bai-Yu Lee,[a] Min Xue,[c] Courtney R. Thomas,[c] Huan Meng,[b] Daniel Ferris,[c] Andre E. Nel,[b,d] Jeffrey I. Zink,[c,d] and Marcus A. Horwitz[a]

Division of Infectious Diseases[a] and Division of NanoMedicine,[b] Department of Medicine, Department of Chemistry & Biochemistry,[c] and California NanoSystems Institute,[d] University of California, Los Angeles, California, USA

Delivery of antituberculosis drugs by nanoparticles offers potential advantages over free drug, including the potential to target specifically the tissues and cells that are infected by *Mycobacterium tuberculosis*, thereby simultaneously increasing therapeutic efficacy and decreasing systemic toxicity, and the capacity for prolonged release of drug, thereby allowing less-frequent dosing. We have employed mesoporous silica nanoparticle (MSNP) drug delivery systems either equipped with a polyethyleneimine (PEI) coating to release rifampin or equipped with cyclodextrin-based pH-operated valves that open only at acidic pH to release isoniazid (INH) into *M. tuberculosis*-infected macrophages. The MSNP are internalized efficiently by human macrophages, traffic to acidified endosomes, and release high concentrations of antituberculosis drugs intracellularly. PEI-coated MSNP show much greater loading of rifampin than uncoated MSNP and much greater efficacy against *M. tuberculosis*-infected macrophages. MSNP were devoid of cytotoxicity at the particle doses employed for drug delivery. Similarly, we have demonstrated that the isoniazid delivered by MSNP equipped with pH-operated nanovalves kill *M. tuberculosis* within macrophages significantly more effectively than an equivalent amount of free drug. These data demonstrate that MSNP provide a versatile platform that can be functionalized to optimize the loading and intracellular release of specific drugs for the treatment of tuberculosis.

Tuberculosis (TB) is one of the leading causes of morbidity and mortality worldwide. According to the World Health Organization, *Mycobacterium tuberculosis*, the causative agent of tuberculosis, infects about one-third of the world's population, and it causes ~9 million new cases of active tuberculosis and 1.7 million deaths annually (38). While effective antibiotics are available, serious toxic side effects limit the doses that can be used clinically. For example, three of the first-line drugs for treating tuberculosis, isoniazid (INH), rifampin (RIF), and pyrazinamide (PZA), are limited by hepatotoxicity (46), a side effect due to the action of the drug on hepatocytes rather than macrophages, the primary host cells that harbor *M. tuberculosis*. Thus, a delivery mechanism that introduces these antibiotics selectively into macrophages would greatly increase their therapeutic index by achieving higher concentrations of the antibiotics locally where *M. tuberculosis* replicates without exposing the patient to high systemic concentrations that cause toxicities. Moreover, because drug resistance develops when bacteria are treated with subtherapeutic levels of antibiotics, a system that allows delivery of high concentrations of antibiotic to the site where bacteria divide would facilitate delivery of sterilizing doses to sites of infection and minimize the emergence of drug resistance. Because *M. tuberculosis* resides and multiplies within host mononuclear phagocytes and because mononuclear phagocytes internalize particles more efficiently than other host cells, encapsulation of antituberculosis drugs within nanoparticles offers a mechanism for specific targeting of *M. tuberculosis*-infected cells. Indeed, because nanoparticles have been shown to be taken up by macrophages of the reticuloendothelial system and to accumulate in the liver, spleen, and lung (8, 21, 25), they are ideally suited to treat *M. tuberculosis*, which infects macrophages in these organs. An additional advantage of nanoparticle delivery of antituberculosis drugs over free drug is that it shields the drug from degradation or modification prior to delivery of the drug to infected tissues.

A variety of different nanoparticles have been tested both *in vitro* and *in vivo* as delivery platforms for antituberculosis drugs (reviewed by Gelperina et al. [17], Griffiths et al. [20], and Sosnik et al. [44]). For example, Anisimova et al. (3) demonstrated that encapsulating INH, streptomycin (STM), and RIF in poly-*n*-butylcyanoacrylate and polyisobutylcyanoacrylate nanoparticles (250-nm average diameter) increased intracellular accumulation of the drugs and decreased the MIC of INH and STM for *M. tuberculosis* by 3- to 4-fold versus that of free drug. Kisich et al. (23) encapsulated moxifloxacin within biodegradable poly(butyl cyanoacrylate) nanoparticles and lowered the MIC for *M. tuberculosis* in macrophages by 10-fold versus that of free drug. Ain et al. reported that encapsulating tuberculosis drugs in alginate- and chitosan-based biodegradable microparticles (90 to 100 μm in diameter) achieved enhanced chemotherapeutic efficacy following oral administration in animal models of tuberculosis (2). Saraogi et al. (40) demonstrated that RIF entrapped within gelatin nanoparticles (264-nm diameter) provided a sustained release of drug after intravenous injection in mice. Sharma et al. (43) used wheat germ agglutinin functionalized poly(lactic-*co*-glycolic acid)

Received 3 November 2011 Returned for modification 24 December 2011
Accepted 9 February 2012
Published ahead of print 21 February 2012
Address correspondence to Marcus A. Horwitz, mhorwitz@mednet.ucla.edu, or Daniel L. Clemens, dclemens@mednet.ucla.edu.

doi:10.1128/AAC.06049-11

(PLGA) nanoparticles for *in vivo* delivery of INH, RIF, and PZA and demonstrated prolonged release of drug, allowing less-frequent dosing to achieve a therapeutic effect in animal models. Muttil et al. (37) administered INH and rifabutin encapsulated within poly(lactic acid) by the aerosol route to mice and reported intramacrophage drug levels 20-fold higher than levels achieved by oral, intravenous, or intratracheal instillation of soluble drug. Finally, Pandey and Khuller (39) administered RIF, INH, and PZA incorporated into solid lipid particles (1 to 2 μm in size) by nebulization to guinea pigs infected with *M. tuberculosis* and achieved a therapeutic effect equivalent to that with daily oral dosing.

While the nanoparticle delivery systems for TB drugs reported to date offer advantages over free drug, they may also be associated with some disadvantages compared with mesoporous silica nanoparticles (MSNP) (4). Liposomes and solid lipid particles have intrinsically poor chemical stability and are degraded by serum (16), thereby decreasing drug delivery to the target cells while increasing potential systemic toxicity. There is also concern that macrophage uptake of biodegradable polymer-based nanoparticles (such as poly-L-lactide and PLGA) may cause cell damage, cytokine release, and inflammation (24, 32, 42), although evidence of their benign nature and lack of associated histopathology has also been reported (11, 41). In contrast to these potential problems with liposomal and biodegradable polymer delivery systems, preliminary *in vivo* experiments have found enhanced blood stability of MSNP compared with liposomes and polymeric nanoparticles (4) and have demonstrated favorable biocompatibility, biodegradation and excretion properties (18, 29, 45).

Whereas the use of liposomes, solid lipid particles, biodegradable nanoparticles, and microspheres for delivery of antituberculosis drugs has been described, the use of MSNP as a delivery platform for antituberculosis drugs has not been reported previously. MSNP are 100-nm-size silica nanoparticles with 2-nm-size pores. These pores run parallel through the MSNP and form a hexagonal pattern. MSNP are attractive delivery vehicles for *M. tuberculosis* drugs because they can be manufactured with a variety of surface and internal functionalizations, allowing incorporation of a variety of different design features (27, 28), especially those that allow controlled release of cargo under specific environmental conditions (10, 13, 15, 35, 50). The biocompatible solid MSNP framework provides intrinsic stability compared with existing liposome-, polymer-, and copolymer-based nanoparticle delivery platforms. In addition, MSNP can be manufactured with a variety of aspect ratios to optimize targeting of the particles to particular organs, tissues, cells, and intracellular environments (12, 19, 22).

To take advantage of the fact that macrophages are particularly efficient in internalizing particles and delivering the particles to acidified endosomes, we have utilized MSNP as a delivery vehicle for two first-line antituberculosis drugs, INH and RIF. The MSNP that we have tested to deliver these drugs are the following: (i) unmodified MSNP (silanol surface); (ii) MSNP surface functionalized with a cationic polyethyleneimine (PEI) (10-kDa) polymer that enhances cellular uptake and lysosomal release while leaving the porous interior free for drug binding and delivery (33, 48); and (iii) MSNP equipped with pH-operated beta-cyclodextrin nanovalves that open and release the cargo molecules in response to endosomal acidification (Fig. 1). We have shown previously that these MSNP with pH-operated nanovalves are responsive to endosomal acidification conditions in human differentiated THP-1 cells (35, 49). Here we show that the MSNP are internalized efficiently by *M. tuberculosis*-infected macrophages, selectively release drugs intracellularly in macrophages, and kill *M. tuberculosis* more effectively than an equivalent amount of free drug. Moreover, we demonstrate that for different antituberculosis drugs, different surface functionalizations of the MSNP yield optimal intracellular killing of *M. tuberculosis* within the infected macrophages, i.e., the optimal surface functionalization is drug specific. In the case of RIF, surface functionalization of the MSNP with 10-kDa PEI yields greater loading and delivery of drug to *M. tuberculosis*-infected macrophages than uncoated MSNP. On the other hand, in the case of INH, MSNP equipped with pH-sensitive valves designed to remain closed at the neutral pH of the blood but to open after endocytosis and acidification of the endosome deliver sterilizing doses of INH within the *M. tuberculosis*-infected macrophage. Thus, we have found that for RIF, optimal loading of MSNP can be achieved by passive design features that optimize phase transfer and electrostatic interactions. On the other hand, for INH, a hydrophilic molecule that does not interact strongly with mesoporous silica, the active feature of a pH-operated gate is required to optimize loading and controlled delivery. This study shows the feasibility of using functionalized MSNP as drug delivery vehicles to improve the treatment of tuberculosis.

MATERIALS AND METHODS

Materials. All chemicals unless specified otherwise were purchased from Sigma-Aldrich. INH and RIF stocks were prepared at 20 mg/ml in dimethyl sulfoxide (DMSO) and stored at −20°C. Phorbol 12-myristate 13-acetate (PMA) was prepared as 100 μM stock in DMSO and stored at −20°C.

Loading MSNP with drugs. The MSNP, PEI-coated MSNP, and nanovalve-equipped MSNP were synthesized according to our previous publication (48). To load RIF, 15 mg of MSNP or PEI-coated MSNP were mixed with 10 mg of RIF in 1 ml methanol, and the mixture was stirred at room temperature for 2 days. The MSNP were then washed with methanol and water. To load INH, 15 mg of nanovalve-equipped MSNP were mixed with 10 mg of INH in 1 ml water. Another 15 mg of nanovalve-equipped MSNP were mixed with 5 ml of 1 mM Hoechst 33342 aqueous solution, serving as the model cargo. The mixture was stirred at room temperature for 24 h, followed by the addition of 10 mg of β-cyclodextrin. The mixture was stirred for another 24 h, and the MSNP were collected via centrifugation and washed with water.

Drug loading and release measurement. To evaluate the pH operation of the nanovalve-equipped MSNP, 5 mg of Hoechst-loaded MSNP were placed in 6 ml of water. A 376-nm laser probe beam was introduced to excite released Hoechst molecules. The change of solution fluorescence was monitored through a time-resolved fluorescence spectrum method.

The release of INH from the nanovalve-equipped MSNP was followed by measuring the absorbance at 260 nm after acidification of the solution with maleic acid.

To evaluate the loading and release capacities of MSNP in the presence of protein, we suspended MSNP loaded with antituberculosis drugs (INH and RIF) in neutral 1% albumin solution, dispersed them using a W-375 sonicator with a micro tip probe (Ultrasonics, Inc.), and centrifuged them at 14,000 × *g* for 10 min to remove drug not bound by the particles. Drugs were then released from the pH-gated nanoparticles by treatment with maleic acid (pH 1.8) for 1 h.

The amount of INH eluted from the MSNP was determined using the salicylaldehyde spectrofluorimetric assay (36). Proteins were removed from the samples by precipitation with 4.5% trichloroacetic acid and centrifugation at 10,000 × *g* for 5 min. Two parts of the clear supernate were mixed with one part of a freshly prepared acetate solution containing 0.5 M sodium acetate, 0.2% (wt/vol) sodium bisulfite, 0.15 M sodium hydroxide, and 0.15% (wt/vol) salicylaldehyde and incubated for 10 min at

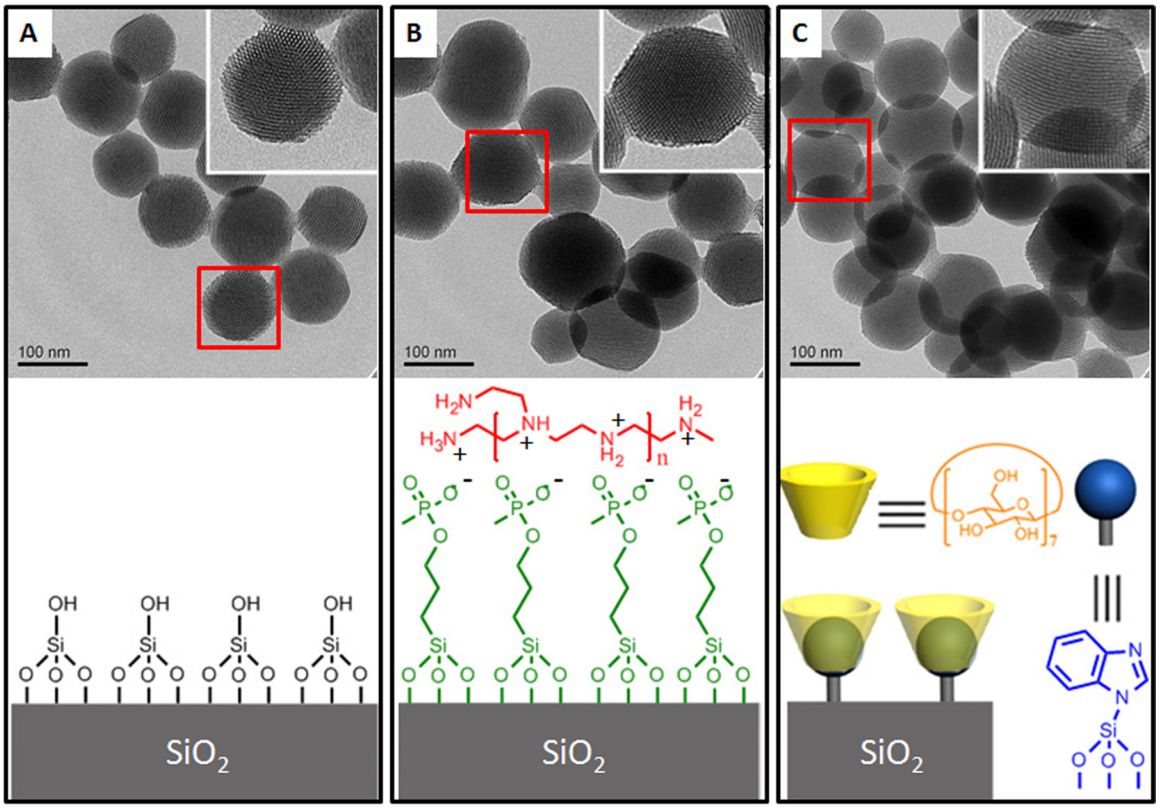

FIG 1 Upper panel: TEM images of MSNP (A), PEI-coated MSNP (B), and MSNP equipped with pH-operated nanovalves (C). The inserts show higher magnification of the particles delineated by red boxes, revealing their pore structure. Lower panel: the surface functionality of each MSNP.

room temperature. A second acetate solution was then added to the sample to achieve a final concentration of 0.25 M sodium acetate, 0.1% sodium bisulfite, and 0.078 M sodium hydroxide. Dithiothreitol (DTT) was added to the samples to a final concentration of 143 mM. The samples were heated at 50°C for 10 min, cooled to room temperature, and extracted with isobutanol. Aliquots (100 μl) of the isobutanol phase were transferred to a 384-well black polypropylene Matriplate (Matrical Bioscience), and the fluorescence intensity was measured using excitation and emission wavelengths of 392 and 478 nm, respectively, in a FlexStation fluorescence plate reader in the UCLA/CNSI Molecular Screening Shared Resource (MSSR) facility. INH standard curves were prepared by the same method.

The amount of RIF loaded on PEI-coated nanoparticles (NP) loaded with RIF (NP-RIF) was determined after elution by spectrophotometric measurement at the wavelength 474 nm against RIF standards. To measure the release of RIF into macrophage cultures, we employed RPMI without a neutral red pH indicator both for the culture of macrophages and to prepare the RIF standards.

Bacteria and cell cultures. The *M. tuberculosis* virulent strain Erdman (35801; American Type Culture Collection) was cultivated on Middlebrook 7H11 agar for 10 days at 37°C in a 5% CO_2–95% air atmosphere. Prior to their use for infection of human macrophages, bacteria were scraped from agar plates and sonicated in a water bath sonicator (Astrason Scientific) for 8 periods of 15 s each to disperse bacterial aggregates. Residual aggregates were removed by 3 sequential centrifugations at 200 g for 10 min at 4°C. The supernate, consisting almost entirely of single bacteria, was used for infection of macrophages. THP-1, a human monocytic cell line (ATCC TIB 202) was maintained in RPMI-1640 (Mediatech) supplemented with 2 mM glutamine, 10% heat-inactivated fetal bovine serum (HI-FBS), and penicillin-streptomycin (100 IU/ml and 100 μg/ml, respectively). Prior to infection with *M. tuberculosis*, THP-1 cells were added to 24-well plates at a concentration of 3×10^5 cells/ml per well and differentiated to a macrophage-like cell type with phorbol myristate acetate (PMA) (100 nM) in RPMI-1640 with 10% HI-FBS for 3 days at 37°C in air containing 5% CO_2. Human peripheral blood monocyte-derived macrophages were prepared as described previously (9). The UCLA Institutional Review Board approved the participation of normal human blood donors in our research.

***M. tuberculosis* killing assay.** PMA-differentiated, human macrophage-like THP-1 cells were infected with *M. tuberculosis* at a ratio of 10 bacteria per cell in RPMI-1640 containing 10% human serum type AB for 90 min at 37°C, 5% CO_2. Extracellular bacteria were removed by washing extensively, and fresh medium with or without nanoparticles and antituberculosis drugs was added. Infected THP-1 cells were incubated for 5 h or 3 days (in the continued presence of the nanoparticles or antituberculosis drugs) and lysed with 0.1% SDS. Culture supernatant and lysed THP-1 cells were combined, serially diluted in 7H9 medium with 10% oleic acid-albumin-dextrose-catalase (OADC) enrichment and 0.05% Tween 80, and plated on 7H11 agar. Bacterial CFU were enumerated after 2 weeks of incubation at 37°C in a 5% CO_2–95% air atmosphere.

Immunofluorescence microscopy. To study whether nanoparticles were delivered to the infected macrophages, we seeded human macrophages on 2-cm coverslips and infected them with *M. tuberculosis* expressing green fluorescent protein as described above. At the end of the 90-min incubation period, monolayers were washed and incubated with fresh medium containing rhodamine isothiocyanate (RITC)-labeled nanoparticles for 90 min to 3 days at 37°C in a 5% CO_2–95% air atmosphere. Macrophages on coverslips were fixed in 4% paraformaldehyde in 0.075 M sodium phosphate buffer, pH 7.4, for 30 min at room temperature, washed with phosphate-buffered saline (PBS), stained with 4′,6-diamidino-2-phenylindole (DAPI), and mounted with Prolong Gold Antifade mounting medium (Invitrogen). To determine whether nanopar-

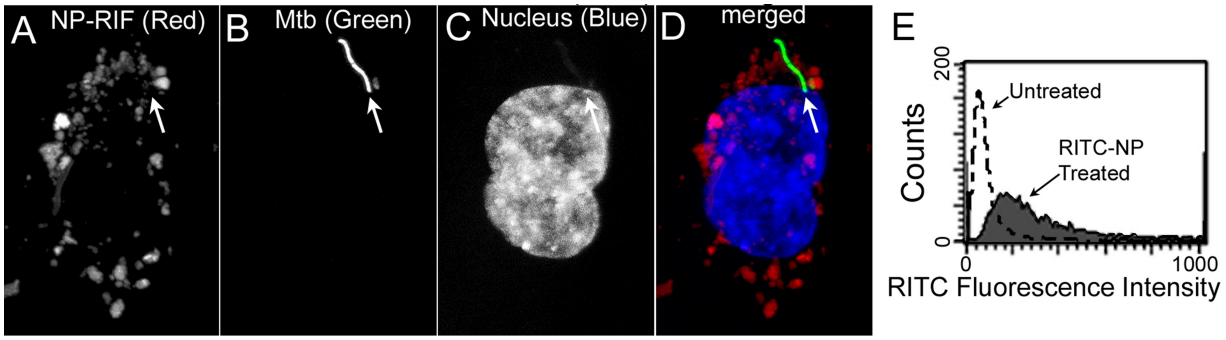

FIG 2 Antituberculosis drug-loaded MSNP are internalized efficiently by human macrophages infected with *M. tuberculosis* (A to D) and by uninfected macrophages (E). PMA-differentiated THP-1 cells were infected with *M. tuberculosis* for 90 min and then incubated with 125 μg/ml NP-RIF. The infected monolayer was fixed 3 days later and analyzed by confocal microscopy. Abundant red fluorescent NP-RIF (A) is seen in the immediate vicinity of the green fluorescent protein-expressing *M. tuberculosis* (arrow) (B) in the infected macrophage, whose nucleus is stained blue (C). The merged image is shown in panel D. We have obtained similar results with human MDM. (E) The macrophage-like THP-1 cells were left untreated (dashed line) or were incubated with 20 μg/ml of fluorescent NP-RIF (RIF-loaded NP) for 6 h (solid line) and then fixed and evaluated by fluorescence-activated cell sorting (FACS). The majority of the macrophages that were incubated with RITC-labeled NP-RIF internalized the fluorescent nanoparticles and exhibited a 10-fold-greater mean fluorescence intensity than the untreated control macrophages.

ticles were delivered to the lysosomes, we incubated macrophages with wheat germ agglutinin (WGA)-Alexa Fluor 633 (5 μg/ml) for 5 min at room temperature to stain plasma membranes, washed with Hanks balanced salt solution, fixed as described above, permeabilized with 0.1% saponin in PBS containing 10 mM glycine, and incubated the macrophage preparation with 1% bovine serum albumin (BSA) in PBS to block nonspecific staining. Coverslips were stained sequentially with (i) mouse monoclonal antibody to human CD63 (University of Iowa Hybridoma Bank) in PBS overnight at 4°C, (ii) Alexa Fluor 555-conjugated goat anti-mouse IgG diluted 1:200 in 1% BSA in PBS for 90 min at room temperature, and (iii) DAPI and then processed with antifade mounting medium as described above. The coverslips were viewed by epifluorescence microscopy with an Eclipse TE2000-S microscope equipped with an X-Cite 120 light source (Nikon), and images were acquired with a SPOT RT-KE monochrome camera and SPOT software (Diagnostic Instruments, Sterling Heights, MI) or by confocal scanning microscopy (Leica confocal SP2 1P-FCS microscope and Leica confocal software in the UCLA/CNSI Advanced Light Microscopy/Spectroscopy Core Facility). To assess colocalization with CD63, we obtained confocal images using an oil immersion 100× objective lens, scanning physical dimensions of 75-μm-by-75-μm areas at a speed of 400 MHz and a resolution of 1,024 × 1,024 pixels. Frame averaging was done with 3 to 4 scans to reduce noise. Nanoparticles were defined as objects with a positive signal in the green channel with an area of at least 4 contiguous pixels and an average pixel intensity of at least 25 units above background on the 0-to-255 scale. A nanoparticle was scored as colocalizing with CD63 if a positive signal in the red channel (average pixel intensity greater than 25 on the 0-to-255 scale) either was superimposed on the position of the nanoparticle or circumferentially rimmed the nanoparticle. Nanoparticles were considered to be within the macrophages if they resided within the WGA-stained contours of the macrophage plasma membrane.

RESULTS

MSNP are taken up efficiently by human macrophages and delivered to lysosomes. MSNP have been shown to be successful platforms for drug delivery *in vitro* and *in vivo* (18, 29, 30, 45, 47, 48, 50). The MSNP used in this study are synthesized through a well-established sol-gel method (27) and use cetyl trimethylammonium bromide as a templating agent. The nanoparticles produced by this process are about 100 nm in diameter and have 2-nm-size parallel pores forming a hexagonal pattern (Fig. 1A). The TEM images of MSNP coated with 10-kDa PEI and MSNP equipped with pH-operated nanovalves are shown in Fig. 1B and C. The pore structure remained intact during the modification process. The PEI polymer was attached on the surface of MSNP through electrostatic interaction with grafted phosphonate groups, while the nanovalves were attached by covalent binding via siloxy bonds.

To demonstrate that MSNP can be adapted as a platform for delivering anti-TB drugs, MSNP were incubated with PMA-differentiated, human macrophage-like THP-1 cells and with human peripheral blood monocyte-derived macrophages (MDM). The results show that MSNP can be internalized efficiently by these cells whether the macrophages are uninfected or infected with *M. tuberculosis* (Fig. 2). We used confocal microscopy to follow the intracellular trafficking of fluorescein isothiocyanate-labeled nanoparticles and their uptake by human THP-1 cells. CD63 (stained with an Alexa Fluor 555-conjugated antibody) was used as a marker of late endosomes and lysosomes, and macrophage plasma membranes were identified by staining with Alexa Fluor 633-conjugated WGA. At 3 h after addition of the MSNP to the macrophages, 94% ± 2% (mean ± standard error) of the intracellular MSNP colocalized with CD63. As an internal control, MSNP that resided outside the WGA-stained contours of the macrophage plasma membranes did not colocalize with CD63 (Fig. 3A to D).

PEI-coated MSNP have a higher RIF loading capacity than uncoated MSNP. In previous studies, MSNP have demonstrated the ability to carry and release hydrophobic drugs *in vitro* and *in vivo* through a phase transfer mechanism (29, 30). RIF is relatively hydrophobic (its solubility in water is 2.5 mg/ml, but that in chloroform is 25 mg/ml) and because of this undergoes a phase transition that preferentially maintains the drug in the porous interior of the MSNP under aqueous conditions, even in the absence of pH-operated gates. We have shown previously (48) that decoration of the negatively charged MSNP surface with positively charged 10-kDa PEI enhances particle uptake and allows cargo to be delivered from acidifying endosomes to the cytosol. PEI-coating of MSNP promotes delivery of drug to the cytosol by a proton sponge mechanism wherein the primary amines of the PEI-MSNP buffer the protons being pumped into the lysosomal compart-

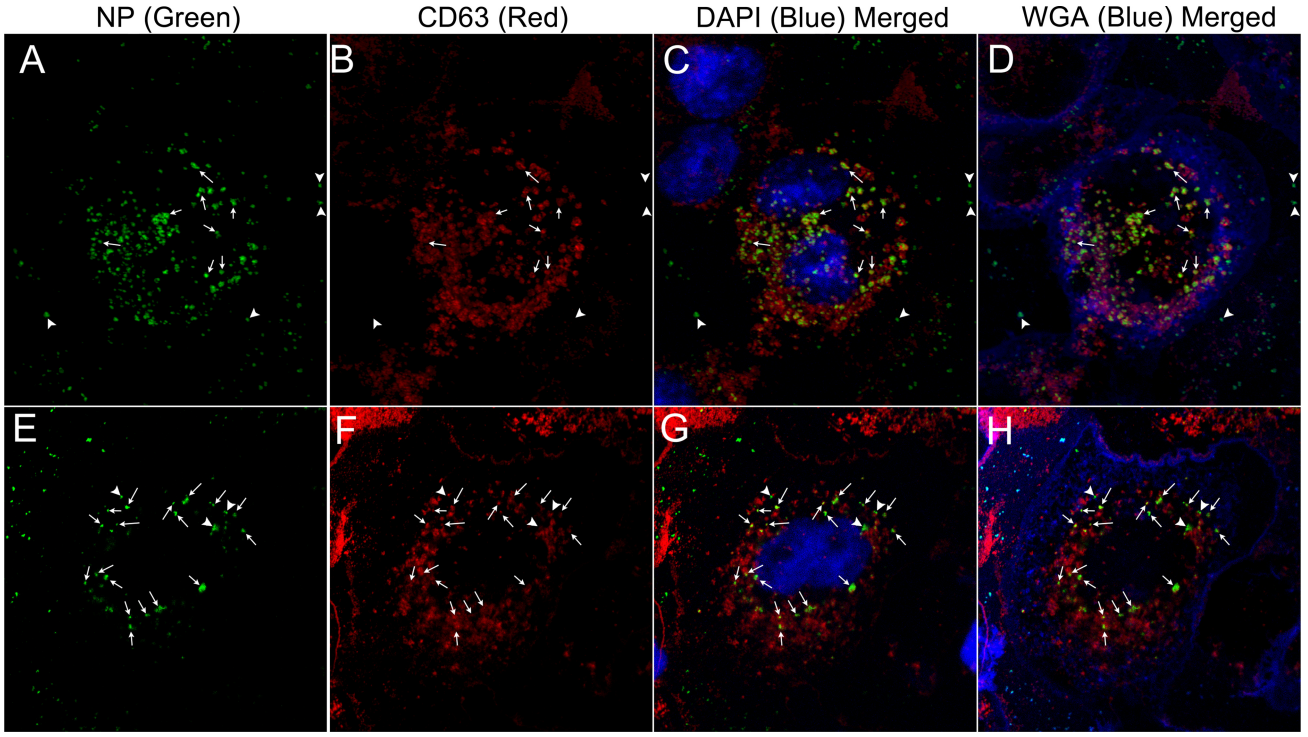

FIG 3 MSNP traffic to lysosomal compartments in human macrophages. THP-1 cells were incubated for 3 h with 15 μg/ml of green fluorescent nanoparticles (uncoated FITC-MSNP [top row, A to D] or PEI-coated FITC-MSNP [bottom row, E to H]). Macrophage plasma membranes were stained with Alexa Fluor 633-WGA (shown as pseudocolor blue in merged images, D and H). After fixation and permeabilization, the late endosomal-lysosomal marker, CD63, was stained with a red fluorescent antibody (B and F), and the macrophage nuclei were stained blue with DAPI (shown in merged images in C and G). Both the uncoated and PEI-coated MSNP (several of which are indicated by arrows) colocalized extensively with CD63 (96% and 89% colocalization, respectively). Several uncoated MSNP located outside the macrophages, indicated by arrowheads (A to D), did not colocalize with CD63. Approximately 11% of intracellular PEI-coated MSNP did not colocalize with CD63 (three noncolocalizing MSNP are indicated by arrowheads; E to H). We have observed a similar high level of colocalization of MSNP with lysosomal compartments in human MDM.

ment by the v-ATPase (proton pump). This leads to heightened pump activity and accumulation of a Cl^- and a water molecule for each proton retained within the compartment, culminating in osmotic rupture of the compartment (5). In addition, we show here that PEI coating of the MSNP increases the amount of RIF that can be delivered by the particles.

We assessed the intracellular trafficking of PEI-coated MSNP by confocal immunofluorescence using the methods described above for uncoated MSNP. As was the case for uncoated MSNP, the intracellular PEI-coated MSNP colocalized extensively with CD63-positive compartments (89% ± 4%, mean ± standard error) 3 h after their addition to the THP-1 macrophages (Fig. 3E to H). PEI-coated MSNP that were outside the macrophages did not colocalize with CD63.

To examine the binding and release of RIF by 10-kDa PEI-coated MSNP and uncoated MSNP, we loaded the particles with RIF and eluted them with the following: (i) water, (ii) 1% BSA in 10 mM HEPES, pH 7.4, (iii) 1% BSA in 0.1 M citrate, pH 5, (iv) DMSO, (v) 1 N HCl in DMSO, or (vi) aqueous 1 N HCl (Fig. 4). Prior to elution, the pelleted particles were visibly stained a dark-red color by RIF (PEI-NP-RIF were obviously darker than the uncoated NP-RIF), and after maximal elution, both types of particles had negligible red staining, indicating an absence of RIF. The amount of RIF released from the particles under various conditions was determined by pelleting the particles at sequential times over a 60-min period and measuring the amount of RIF in the

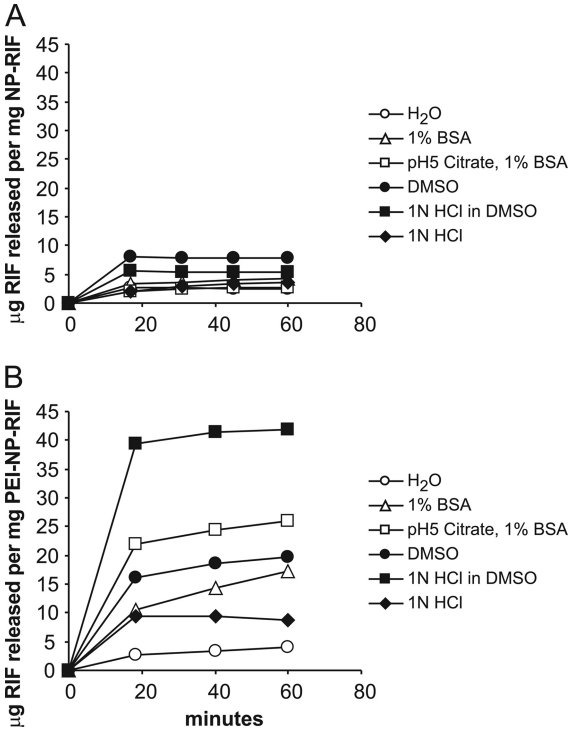

FIG 4 Time course release of RIF from uncoated MSNP (A) or PEI-coated (B) MSNP.

supernate by UV-visible (UV-vis) spectroscopy. In the case of uncoated NP-RIF, maximum release (0.79% [wt/wt]) was achieved with DMSO within 20 min, and treatment with acidified DMSO did not elute any additional RIF. In the case of PEI-NP-RIF, release of RIF also plateaued within 20 min, but more RIF was released by acidified DMSO (42 μg/mg PEI-NP-RIF at 60 min or 4.2% [wt/wt]) than by nonacidified DMSO (2.0% [wt/wt]). These results indicate that the PEI coating of the MSNP increased its binding capacity for RIF by 5-fold compared with uncoated MSNP.

We found that under abiotic conditions, a hydrophobic solvent such as DMSO was required for complete elution of RIF from the PEI-NP-RIF. In these experiments, DMSO was chosen as a hydrophobic solvent for eluting RIF from the MSNP because RIF is freely soluble in DMSO and its use permits an assessment of the total amount of drug that can be eluted from the MSNP. While DMSO does not reflect a physiological condition, it may simulate hydrophobic environments found within the macrophage, such as within the membrane lipids of the endosomal-lysosomal system and in multivesicular bodies of secondary lysosomes. Our findings in this study are consistent with our previously published observations that MSNP are capable of loading and releasing water-insoluble drugs (e.g., paclitaxel and camptothecin) by a phase transfer mechanism that can be reversed by ethanol washing of the particles, thus demonstrating the role of hydrophobicity in MSNP drug entrapment (29, 30, 33).

The efficacy of PEI-coated NP-RIF in killing *M. tuberculosis* within human macrophages is greater than those of NP-RIF and free RIF. To evaluate the efficacy of RIF-loaded nanoparticles in killing intracellular *M. tuberculosis* in infected macrophages, we incubated monolayers of PMA-differentiated THP-1 cells in 24-well plates with the virulent *M. tuberculosis* Erdman strain for 90 min at a multiplicity of infection of 10:1 (bacteria/macrophage), washed away the extracellular bacteria, and added fresh medium containing NP-RIF, PEI-NP-RIF, or known amounts of free RIF. As a control for free RIF present in the NP-RIF and PEI-NP-RIF conditions, the suspensions of extensively washed drug-loaded NP (in 1% BSA) were pelleted by centrifugation and the supernatant solutions were added to monolayers of *M. tuberculosis*-infected THP-1 cells. The RIF present in these controls (referred to as "unbound RIF") reflects RIF eluted in the neutral 1% BSA solution. Compared with either no treatment or treatment with control nanoparticles (containing no drug), treatment of *M. tuberculosis*-infected THP-1 cells with either MSNP or PEI-coated MSNP loaded with RIF reduced the number of intracellular bacteria over a 3-day treatment and yielded greater killing than the corresponding "unbound RIF" controls. Consistent with its greater capacity to bind and deliver RIF, PEI-NP-RIF killed intracellular *M. tuberculosis* more effectively than an equivalent amount of NP-RIF (Fig. 5). Treatment of the infected monolayers with PEI-NP-RIF for 3 days at a concentration of 15.6 μg/ml reduced CFU of intracellular *M. tuberculosis* by 1.6 logs compared with controls versus only 0.3 logs for NP-RIF, and treatment with 62.5 μg/ml PEI-NP-RIF reduced CFU by 3.3 logs, versus only 1.2 logs for NP-RIF (Fig. 5 B and C).

We added known amounts of free RIF to *M. tuberculosis*-infected THP-1 monolayers to generate a RIF bioassay standard curve (Fig. 5A) and compared the effectiveness of nanoparticle-delivered RIF (Fig. 5B and C) to that of free RIF in killing *M. tuberculosis* in infected THP-1 cells. The upper dose of RIF used in the standard curve, 5 μg/ml, is comparable to therapeutic blood levels of RIF (1). We found that the extent of bacterial killing achieved with 62.5 μg/ml NP-RIF was equivalent to that achieved with 0.44 μg/ml of free RIF. From our spectrometric release assay, we have determined that the uncoated MSNP have a RIF loading capacity of 0.79% on a weight basis, equivalent to 0.49 μg/ml of elutable RIF from 62.5 μg/ml NP-RIF. Therefore, the efficacy ratio of uncoated NP-RIF (0.49 μg/ml) to free RIF (0.44 μg/ml) is close to 1:1. On the other hand, PEI-NP-RIF at a concentration of 15.6 μg/ml reduced CFU of intracellular *M. tuberculosis* by 1.6 logs, a level of killing that corresponded to 1.1 μg/ml of free RIF. Because PEI-NP has a RIF loading capacity of 4.2% on a weight basis, the amount of elutable RIF from 15.6 μg/ml of PEI-NP-RIF is 0.65 μg/ml, indicating that the efficacy ratio of PEI-NP-RIF to free RIF is ~2:1 (1.1 μg/ml:0.65 μg/ml). PEI-NP-RIF at a concentration of 31.25 μg/ml yielded 2.3 logs of bacterial killing, which corresponds to the bactericidal activity of 4.7 μg/ml of free RIF. At the PEI-NP-RIF loading capacity of 4.2%, the amount of elutable RIF from 31.25 μg/ml of PEI-NP-RIF is calculated to be 1.3 μg/ml, indicating an efficacy ratio of PEI-NP-RIF to free RIF of almost 4:1 (4.7 μg/ml:1.3 μg/ml). Therefore, RIF delivered by PEI-coated MSNP kills intracellular *M. tuberculosis* 2- to 4-fold more effectively than an equivalent amount of free RIF.

Use of MSNP equipped with a pH-sensitive valve as a delivery platform for the antituberculosis drug INH. Whereas RIF has hydrophobic and electrostatic properties that allow it to be loaded efficiently into MSNP by passive phase transfer and electrostatic interactions, INH is a small hydrophilic molecule that under physiological conditions does not interact with mesoporous silica either by phase transitions or by electrostatic interactions. Instead, optimal loading and delivery of INH by MSNP requires mechanization of the MSNP with design features that enable active trapping and controlled release of the cargo molecule. To optimize loading and achieve specific intracellular delivery of drug, we have equipped the MSNP with pH-operated nanovalves (35) (Fig. 6A). The nanovalves function as a gatekeeper to contain the hydrophilic drug molecules within the pores at neutral pH and release the drug from the pores when the pH decreases after the MSNP are internalized by macrophages and traffic to acidified endosomes. We have previously shown that the pH-gated MSNP colocalize extensively (>80%) with acidified lysosomes after their uptake by differentiated THP-1 cells (35).

We utilized the fluorescent dye Hoechst 33342 as a model cargo to demonstrate the pH-dependent operation of the nanovalve-equipped MSNP. Time-resolved fluorescence spectroscopy demonstrated the pH-dependent release of Hoechst 33342 from the nanovalve-equipped MSNP over time (Fig. 6B).

To assess the time course of the pH-dependent release of INH from nanovalve-equipped MSNP, we loaded the particles with INH at neutral pH and then followed the release of the drug by spectrophotometry in the presence of 10 mM maleic acid (pH 1.8). Figure 6C demonstrates that drug release from the nanoparticles plateaus by 50 min.

pH-gated NP-INH kills *M. tuberculosis* in human macrophages more effectively than free INH. Strategies similar to those used to evaluate RIF-loaded MSNP were employed to evaluate the drug delivery and *M. tuberculosis* killing efficacy of pH-gated nanoparticles loaded with INH (NP-INH). To allow us to compare the effectiveness of drug delivered by nanoparticles with that of the free drug, we first eluted INH from pH-gated NP-INH by

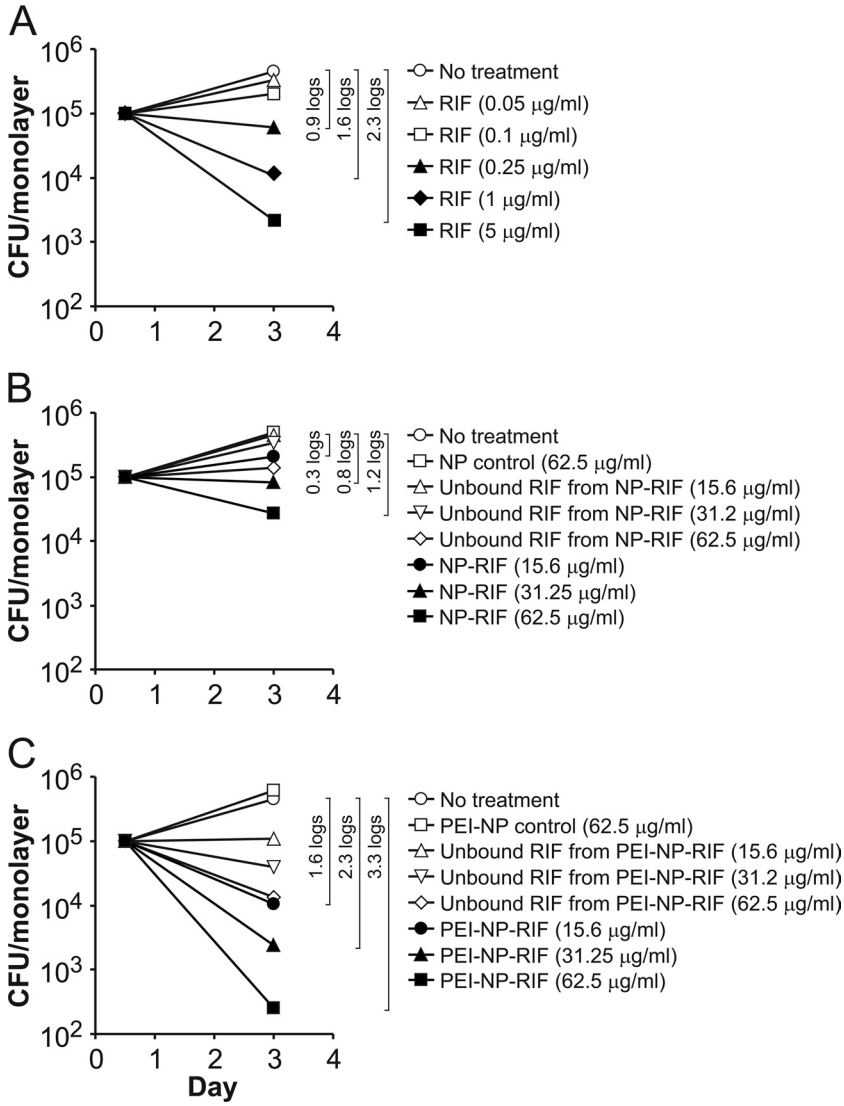

FIG 5 PEI coating on MSNP enhances the delivery of RIF to *M. tuberculosis*-infected human macrophages. PMA-differentiated THP-1 cells were infected with *M. tuberculosis* for 90 min and subsequently treated with free RIF (A), NP-RIF (B), or PEI-NP-RIF (C). CFU of *M. tuberculosis* from the infected macrophage monolayer were enumerated 3 days postinfection. Log differences in CFU/monolayer between the no-treatment condition and selected treatments are indicated within brackets. All differences indicated by brackets were statistically significant at $P < 0.01$ (analysis by one-factor ANOVA).

treatment of the particles with 10 mM maleic acid for 1 h to elute all of the drug. As shown in Fig. 6C, elution of INH from the pH-gated NP reaches a plateau by 50 min. This acid eluate was then neutralized to pH 7.4 with a small amount of Tris base for subsequent addition to monolayers of *M. tuberculosis*-infected macrophages as a control for adding soluble INH to the monolayers. Treatment of INH at pH 1.8 for 1 h does not decrease its antimicrobial activity, as demonstrated in Fig. 7A. We also eluted NP-INH with 1% BSA at neutral pH to assay the effect of the neutral eluate. We quantitated the release of INH from pH-gated NP-INH both with a salicylaldehyde spectrofluorimetric assay and with an *M. tuberculosis* killing bioassay in which we added known amounts of free INH to *M. tuberculosis*-infected THP-1 monolayers to generate a standard curve for INH killing of intracellular *M. tuberculosis*. Both methods gave similar results: the amount of INH eluted from pH-gated NP-INH with 1% BSA was 0.018% on a wt/wt basis (i.e., 180 ng of INH per mg of pH-gated NP-INH) by the spectrophotometric assay and 0.013% (wt/wt) by the bioassay. In contrast, treatment of pH-gated NP-INH with pH 1.8 maleic acid released 0.048% INH (wt/wt) as measured by the spectrophotometric assay and 0.036% (wt/wt) as measured by the bioassay.

When pH-gated NP-INH (250 μg/ml) and control preparations were added to *M. tuberculosis*-infected macrophages for 3 days, no *M. tuberculosis* was detected in the monolayers treated with pH-gated NP-INH, indicating sterilization of the monolayers (i.e., CFU were below our detection limit of 50 CFU/monolayer). Thus, as shown in Fig. 7C, pH-gated NP-INH reduced CFU of intracellular *M. tuberculosis* by at least 3.8 logs compared with no treatment ($P < 0.001$, one-factor analysis of variance [ANOVA]) and yielded 1.5 logs more killing of intracellular *M. tuberculosis* than an equivalent amount of free INH (approxi-

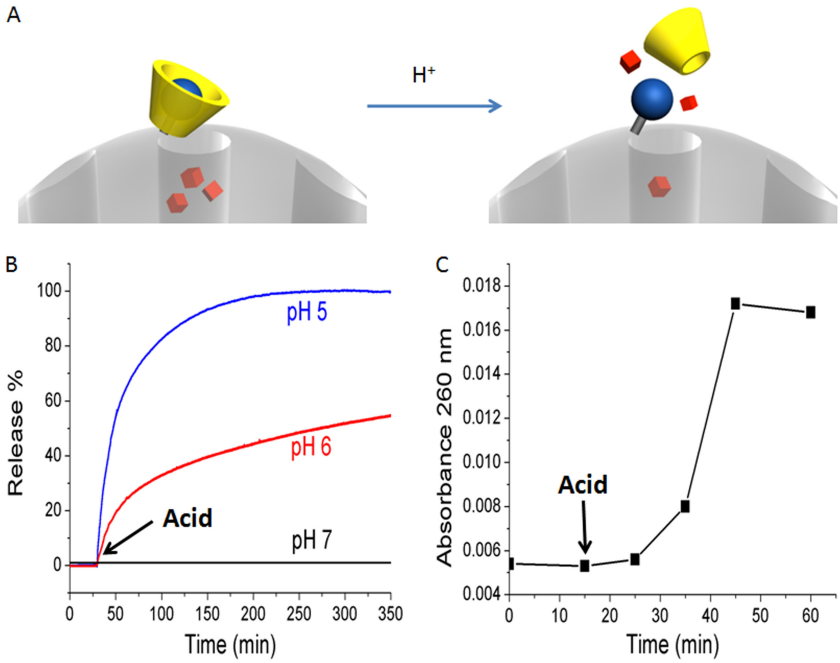

FIG 6 MSNP equipped with pH-sensitive valves as a nanodelivery platform for antituberculosis drugs. (A) Illustration of the principle by which the pH-sensitive valve is operated. (B) Release profiles of Hoechst 33342 dye. The pH-dependent release mechanism can be monitored using this model cargo. Acid was added at 30 min to adjust the solution pH. (C) Time course release of the antituberculosis drug INH from the particles after change from neutral pH to pH 1.8. Acid was added at 15 min to adjust the solution pH.

mately 100 ng/ml), i.e., the acid eluate from the pH-gated NP-INH ($P < 0.01$). In addition, pH-gated NP-INH yielded almost 3 logs more killing than the neutral eluate from an equivalent amount of pH-gated NP-INH ($P < 0.001$, one-factor ANOVA), consistent with a relatively low level of leakage of drug from the pH-gated MSNP at neutral pH (Fig. 7C).

We observed a low level of killing of *M. tuberculosis* with the neutral eluate of the pH-gated NP-INH, consistent with a low level of elution of INH from the pH-gated NP under neutral-pH conditions. While elution of the Hoechst 3342 was not detected from the NP under neutral-pH conditions, we have consistently observed a small degree of elution of INH from the pH-gated NP with neutral-pH solutions that contain serum albumin. The physical chemical properties (e.g., molecular weight, pK_a, and functional groups) of Hoechst 3342 differ markedly from those of INH, and therefore it is not surprising that the two molecules behave somewhat differently with regard to their interactions with pH-gated MSNP. The low level of INH eluted from the pH-gated NP at neutral pH may reflect elution by albumin acting as a chaperone molecule for INH that is weakly bound to the exterior of the NP or bound to the molecular threads or β-cyclodextrin caps of the pH-operated gates. The amount of INH eluted from the NP under these conditions is 3-fold less than the amount of drug that is eluted from the particles in an acidic environment, and accordingly, the killing of *M. tuberculosis* by the neutral-pH eluate was 1.4 logs less than that with the acid eluate of the NP.

DISCUSSION

RIF is an inhibitor of bacterial RNA polymerase. INH is a prodrug that, once activated inside tubercle bacilli, kills the actively growing organisms by inhibiting their cell wall synthesis. Both are among the most commonly used first-line drugs for treating tuberculosis. Systemic administration of both drugs can be complicated by off-target toxicities to cells and tissues that are not infected by *M. tuberculosis*. Delivery of antituberculosis drugs via nanoparticles directly to the cells and tissues that are infected by *M. tuberculosis* has the potential to maximize efficacy and minimize toxicity. To demonstrate the promise of MSNP as a delivery platform for RIF and INH, we delivered these two drugs using MSNP with a surface functionalization specifically tailored to each drug and showed that each MSNP-TB drug formulation led to killing of intracellular *M. tuberculosis* in infected macrophages, providing proof of principle for this technology.

RIF exhibits marked hydrophobicity and undergoes a phase transition that preferentially maintains the drug in the porous interior of the MSNP under aqueous conditions. Despite the fact that unmodified MSNP can be used to deliver RIF, they have a relatively low loading capacity, which limits their potential for treating *M. tuberculosis*. Decoration of the particle surface with a positive charge, such as 10-kDa PEI, enhances particle uptake and facilitates escape of molecules from acidifying endosomes into the cytoplasm (14, 48). In addition, the polymer coating can potentially increase the loading capacity of the MSNP, since some of the drug can be held in the polymer layer. Although RIF is very hydrophobic and is more soluble in chloroform than in water, at neutral pH it is a zwitterion with an isoelectric point of 4.8. It has two ionization constants (pK_a), one at pH 1.7, related to deprotonation of the phenolic hydroxyl group at position C-8, and one at pH 7.9, related to gain of a proton by the N-4 piperazine group (31). Because of its zwitterionic nature, at neutral pH RIF binds to positively charged polymers, such as chitosan (6), thus accounting for the greater loading of RIF onto PEI-coated MSNP than onto uncoated MSNP. Whereas the binding of RIF to uncoated MSNP

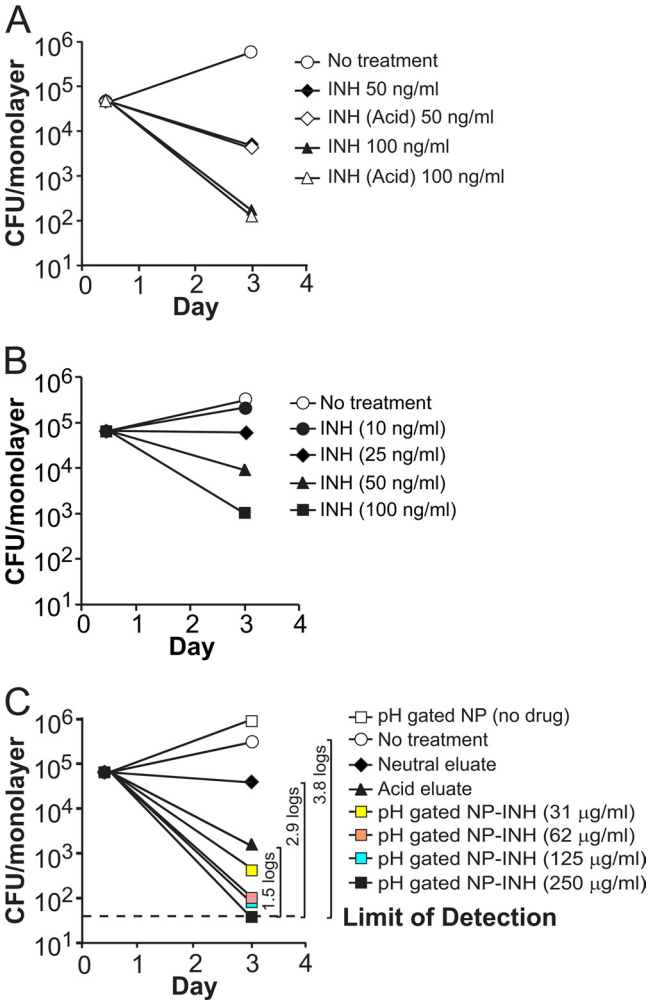

FIG 7 pH-gated NP loaded with INH kill *M. tuberculosis* in human macrophages. PMA-differentiated THP-1 cells were incubated with *M. tuberculosis* for 90 min and then treated with free INH (A and B) or pH-gated NP-INH at concentrations of 31 to 250 μg/ml (C). CFU of *M. tuberculosis* in treated or untreated infected macrophages were enumerated 3 days postinfection. Neutral and acid eluates from 250 μg/ml pH-gated NP-INH served as controls for the amount of INH leakage at neutral pH and INH loading on the particles, respectively. Acid treatment of INH had no effect on its antimycobacterial activity (A). Log differences in CFU/monolayer between the no-treatment condition and selected treatment conditions are indicated within brackets (C). The differences between results for the pH-gated NP-INH-treated monolayer and no treatment and between pH-gated NP-INH and neutral eluate were significant at the $P < 0.001$ level (one-factor ANOVA). The difference between the 250 μg/ml pH-gated NP-INH-treated monolayer and the acid eluate treated monolayer was significant at the $P < 0.01$ level (one-factor ANOVA).

involves primarily hydrophobic interactions, the binding of RIF to PEI-MSNP involves both hydrophobic and ionic interactions. For *in vivo* delivery, use of PEI-coated NP-RIF would confer two advantages over that of uncoated NP-RIF: increased binding/loading of RIF (allowing administration of smaller doses of NP-RIF) and increased uptake by macrophages. In our experiments in which the NP-RIF was allowed to incubate for 3 days with *M. tuberculosis*-infected macrophages, the rate of uptake of drug-loaded MSNP is not a limiting factor. However, in the case of *in vivo* administration, the rate of uptake of the MSNP by macrophages may have a greater impact on the effectiveness of the delivery platform and the advantage of PEI-NP-RIF over NP-RIF may be even more apparent.

We have shown that the effectiveness of PEI-coated MSNP-RIF in killing of intracellular *M. tuberculosis* is 2- to 4-fold greater than that of an equivalent amount free RIF added to the *M. tuberculosis*-infected macrophages. This is consistent with the release of RIF from drug-loaded MSNP within the macrophages causing higher intracellular concentrations of RIF at the site of the intracellular *M. tuberculosis*. The pharmacodynamic advantage of nanoparticle delivery of RIF may be even greater *in vivo* than in our *in vitro* experiments, since the free RIF *in vivo* would have a much greater volume of distribution and would be rapidly cleared (as opposed to the situation in the culture well, where there is a very small volume of distribution and no clearance). Unlike free RIF, in an *in vivo* situation, MSNP-bound RIF would initially be released at the sites of *M. tuberculosis* infection, thereby leading, at least transiently, to locally higher concentrations of drug in *M. tuberculosis*-infected cells and tissues.

While we have observed that MSNP are efficiently internalized by *M. tuberculosis*-infected macrophages, we have found that the MSNP only rarely colocalize with the *M. tuberculosis* bacilli. Therefore, the enhanced efficacy of PEI-NP-RIF over an equivalent amount of free RIF reflects a higher local concentration of RIF within the cell rather than direct delivery of drug to the subcellular compartment occupied by *M. tuberculosis.* Whereas PEI-coated NP-RIF was more effective in killing intracellular *M. tuberculosis* than an equivalent amount of free RIF, we observed comparable killing efficacies by uncoated NP-RIF and an equivalent amount of free RIF. The absence of any increase in efficacy by uncoated-MSNP delivery of RIF might be due to trapping of some of the NP-delivered RIF within lysosomes. This trapping would be overcome by the PEI coating, since PEI promotes release of drugs from acidified lysosomes.

In contrast to RIF, INH is hydrophilic, and we found that a nanovalve modification of the MSNP was necessary for effective drug loading and targeted intracellular delivery. The nanovalves were designed to remain closed under neutral pH and open only in acidic environments, such as acidifying endosomal/lysosomal compartments in cells. The pH-operated nanovalves were constructed by covalent attachment of molecular threads over the pores and addition of bulky β-cyclodextrin molecules that at neutral pH bind to the threads and sterically block the pores. At acidic pH, the molecular threads are protonated, which decreases the binding affinity of the β-cyclodextrin capping molecules for the threads, such that the nanovalves open and allow release of drug molecules from the MSNP (35). In this article, both a fluorimetric assay and a bioassay measured relatively small amounts of INH in the BSA neutral eluate of the pH-gated NP-INH, confirming the pH-controlled release of drug from the MSNP. The fact that we observed only a low level of leakage of INH from the drug-loaded nanoparticles into neutral-pH solutions indicates that systemic administration of INH via the pH-gated NP platform has the potential to deliver the drugs primarily to macrophages, the primary host cells for *M. tuberculosis*, and to minimize off-target toxicity (e.g., to the liver and nervous system) that otherwise complicates the systemic administration of INH. For therapeutic *in vivo* use, the pH-gated NP could be administered by the intravenous route and/or aerosol route. For potential oral use, the pH-gated NP would need to be delivered in such a way, e.g., in low-pH-resistant capsules, as to allow them to transit the stomach to the intestine

without exposure to the acidic environment of the stomach and subsequently to be taken up and transcytosed to the bloodstream without exposure to pH conditions sufficiently low to open the gates and release drug. The oral delivery of drugs via NP is a field still in its infancy, and new advances will be necessary to achieve efficient oral delivery of NP-loaded drugs.

The absolute amount of acid-elutable INH loaded onto the pH-gated NP (approximately 0.05% [wt/wt]) was lower than desired and represents an opportunity for improvement by modifications of the NP design. Nevertheless, our demonstration that INH delivered by pH-gated NP-INH kills 1.5 logs more intracellular *M. tuberculosis* than an equivalent amount of free INH added to the *M. tuberculosis*-infected macrophages provides proof of concept for this approach and justifies further development of this pH-gated MSNP platform. The relative efficacy of pH-gated NP-INH over that of free INH is likely to be even greater in an *in vivo* animal or human tuberculosis infection, where the majority of the systemically administered free INH is rapidly cleared or metabolized without ever being taken up by infected macrophages.

MSNP represent a promising nanocarrier delivery system with great translational potential. The *in vivo* safety of long-term repeated administration of MSNP (e.g., over a period of several months), as may be required for treatment of tuberculosis, has not been determined and requires further study. The tolerability is likely to be related to the route and dose and the particular physicochemical properties of the MSNP administered. In a comprehensive safety assessment that included animal body weight, blood biochemistry, and histological analysis of major organs, we have recently shown that MSNP fail to induce adverse effects after intravenous injection (34). Moreover, MSNP do not damage red cell membranes when a hemolysis assay is used (34). While it is well known that cationic nanoparticles (e.g., PEI-coated MSNP) can induce cytotoxicity, we have previously shown that the cytotoxicity depends on the polymer length and the cationic charge density on the particle. Thus, while high-molecular-weight PEI polymers (e.g., 25-kDa PEI) can induce cytotoxicity in a variety of cell types, we have previously shown (48) that there is no generation of cellular toxicity by the low-molecular-weight polymer (e.g., PEI of $\leq$10 kDa) employed in this study. It is also noteworthy that while MSNP coated with the 25-kDa PEI polymer is cytotoxic *in vitro*, intravenous injection in mice did not elicit any significant toxicity in our previous study (48). One possible explanation for this is that the organs of the reticulo-endothelial system (e.g., the liver and spleen) are highly adept in dealing with particulate matter that can be efficiently removed by protective mechanisms via hepatobiliary transfer (45).

An important consideration related to the safety of MSNP-based therapy is that previous studies have shown that the MSNP do not persist indefinitely but are instead degraded and excreted (26). Abiotic studies in simulated body fluids have demonstrated a gradual decomposition of MSNP, including a breakdown of their architecture and decrease in their surface area (7). *In vivo* studies have confirmed gradual breakdown and excretion. For example, Lu et al. (29) tracked elemental Si following intravenous injection of MSNP and demonstrated that ~94% of the MSNP bolus was recovered in the urine and feces within 4 days of administration. This is in agreement with the demonstration by Souris et al. (45) of the rapid bioelimination of MSNP through hepatobiliary excretion in murine experiments. This constitutes an important safety feature of a nanocarrier that can be either degraded *in situ* in subcellular compartments or excreted from the body once the carrier has served its therapeutic purpose.

While our intent in the present work has been to assess the feasibility of MSNP delivery of drugs that are effective against active tuberculosis, we would anticipate that similar MSNP delivery vehicles loaded with drugs considered active against latent tuberculosis (such as rifapentine, moxifloxacin, and PA-824) could be used to achieve higher intramacrophage concentrations of these drugs and greater efficacy than that of free drug in treating latent TB.

ACKNOWLEDGMENTS

We thank Sarah McNees for technical assistance. We thank the UCLA Molecular Screening Shared Resources and the Advanced Light Microscopy Facility in the UCLA/CNSI for providing equipment, training, and assistance in the use of fluorescence plate reader equipment and confocal microscopy equipment. We thank Travis Pecorelli for assistance in UV-vis measurements and Yuen Lau and Zongxi Li for valuable discussions.

This work was supported by Grand Challenges Explorations Grant 53292 from the Bill and Melinda Gates Foundation and National Institutes of Health grant CA 133697.

REFERENCES

1. **Acocella G, et al.** 1972. Kinetics of rifampicin and isoniazid administered alone and in combination to normal subjects and patients with liver disease. Gut **13**:47–53.
2. **Ain Q, Sharma S, Khuller GK, Garg SK.** 2003. Alginate based oral drug delivery system for tuberculosis: pharmacokinetics and therapeutic effects. J. Antimicrob. Chemother. **51**:931–938.
3. **Anisimova YV, Gelperina SI, Peloquin CA, Heifets LB.** 2000. Nanoparticles as antituberculosis drugs carriers: effect on activity against *Mycobacterium tuberculosis* in human monocyte-derived macrophages. J. Nanopart. Res. **2**:165–171.
4. **Barbé C, et al.** 2004. Silica particles: a novel drug-delivery system. Adv. Mater. **16**:1959–1966.
5. **Boussif O, et al.** 1995. A versatile vector for gene and oligonucleotide transfer into cells in culture and in vivo: polyethylenimine. Proc. Natl. Acad. Sci. U. S. A. **92**:7297–7301.
6. **Cao Z, Sun Y.** 2009. Chitosan-based rechargeable long-term antimicrobial and biofilm-controlling systems. J. Biomed. Mater. Res. A **89**:960–967.
7. **Cauda V, Schlossbauer A, Bein T.** 2010. Bio-degradation study of colloidal mesoporous silica nanoparticles: effect of surface functionalization with organo-silanes and poly(ethylene glycol). Microporous Mesoporous Mater. **132**:60–71.
8. **Chen H, et al.** 2010. Reducing non-specific binding and uptake of nanoparticles and improving cell targeting with an antifouling PEO-*b*-PγMPS copolymer coating. Biomaterials **31**:5397–5407.
9. **Clemens DL, Lee BY, Horwitz MA.** 2004. Virulent and avirulent strains of *Francisella tularensis* prevent acidification and maturation of their phagosomes and escape into the cytoplasm in human macrophages. Infect. Immun. **72**:3204–3217.
10. **Coti KK, et al.** 2009. Mechanised nanoparticles for drug delivery. Nanoscale **1**:16–39.
11. **Dailey LA, et al.** 2006. Investigation of the proinflammatory potential of biodegradable nanoparticle drug delivery systems in the lung. Toxicol. Appl. Pharmacol. **215**:100–108.
12. **Devarajan PV, et al.** 2010. Particle shape: a new design parameter for passive targeting in splenotropic drug delivery. J. Pharm. Sci. **99**:2576–2581.
13. **Du L, Liao S, Khatib HA, Stoddart JF, Zink JI.** 2009. Controlled-access hollow mechanized silica nanocontainers. J. Am. Chem. Soc. **131**:15136–15142.
14. **Duan H, Nie S.** 2007. Cell-penetrating quantum dots based on multivalent and endosome-disrupting surface coatings. J. Am. Chem. Soc. **129**:3333–3338.
15. **Ferris DP, et al.** 2009. Light-operated mechanized nanoparticles. J. Am. Chem. Soc. **131**:1686–1688.
16. **Foradada M, Pujol MD, Bermudez J, Estelrich J.** 2000. Chemical deg-

radation of liposomes by serum components detected by NMR. Chem. Phys. Lipids **104**:133–148.
17. **Gelperina S, Kisich K, Iseman MD, Heifets L.** 2005. The potential advantages of nanoparticle drug delivery systems in chemotherapy of tuberculosis. Am. J. Respir. Crit. Care Med. **172**:1487–1490.
18. **Giri S, Trewyn BG, Lin VS.** 2007. Mesoporous silica nanomaterial-based biotechnological and biomedical delivery systems. Nanomedicine (Lond.) **2**:99–111.
19. **Gratton SE, et al.** 2008. The effect of particle design on cellular internalization pathways. Proc. Natl. Acad. Sci. U. S. A. **105**:11613–11618.
20. **Griffiths G, Nystrom B, Sable SB, Khuller GK.** 2010. Nanobead-based interventions for the treatment and prevention of tuberculosis. Nat. Rev. Microbiol. **8**:827–834.
21. **He Q, Zhang Z, Gao F, Li Y, Shi J.** 2011. In vivo biodistribution and urinary excretion of mesoporous silica nanoparticles: effects of particle size and PEGylation. Small **7**:271–280.
22. **Huang X, Teng X, Chen D, Tang F, He J.** 2010. The effect of the shape of mesoporous silica nanoparticles on cellular uptake and cell function. Biomaterials **31**:438–448.
23. **Kisich KO, et al.** 2007. Encapsulation of moxifloxacin within poly(butyl cyanoacrylate) nanoparticles enhances efficacy against intracellular *Mycobacterium tuberculosis.* Int. J. Pharm. **345**:154–162.
24. **Lam KH, Schakenraad JM, Esselbrugge H, Feijen J, Nieuwenhuis P.** 1993. The effect of phagocytosis of poly(L-lactic acid) fragments on cellular morphology and viability. J. Biomed. Mater. Res. **27**:1569–1577.
25. **Lee JE, et al.** 2010. Uniform mesoporous dye-doped silica nanoparticles decorated with multiple magnetite nanocrystals for simultaneous enhanced magnetic resonance imaging, fluorescence imaging, and drug delivery. J. Am. Chem. Soc. **132**:552–557.
26. **Lin VS.** 2009. Nanomedicine: veni, vidi, vici and then . . . vanished. Nat. Mater. **8**:252–253.
27. **Liong M, et al.** 2009. Mesostructured multifunctional nanoparticles for imaging and drug delivery. J. Mater. Chem. **19**:6251–6257.
28. **Liong M, et al.** 2008. Multifunctional inorganic nanoparticles for imaging, targeting, and drug delivery. ACS Nano **2**:889–896.
29. **Lu J, Liong M, Li Z, Zink JI, Tamanoi F.** 2010. Biocompatibility, biodistribution, and drug-delivery efficiency of mesoporous silica nanoparticles for cancer therapy in animals. Small **6**:1794–1805.
30. **Lu J, Liong M, Zink JI, Tamanoi F.** 2007. Mesoporous silica nanoparticles as a delivery system for hydrophobic anticancer drugs. Small **3**:1341–1346.
31. **Malabarba A, Ferrari P, Depaoli A, Gallo GG, Cavalleri B.** 1986. Synthesis and conformation of some acetyl derivatives of rifampicin. Farmaco Sci. **41**:131–150.
32. **Marques AP, Reis RL, Hunt JA.** 2004. Cytokine secretion from mononuclear cells cultured in vitro with starch-based polymers and poly-L-lactide. J. Biomed. Mater. Res. A **71**:419–429.
33. **Meng H, et al.** 2010. Engineered design of mesoporous silica nanoparticles to deliver doxorubicin and P-glycoprotein siRNA to overcome drug resistance in a cancer cell line. ACS Nano **4**:4539–4550.
34. **Meng H, et al.** 2011. Use of size and a copolymer design feature to improve the biodistribution and the enhanced permeability and retention effect of doxorubicin-loaded mesoporous silica nanoparticles in a murine xenograft tumor model. ACS Nano **5**:4131–4144.
35. **Meng H, et al.** 2010. Autonomous in vitro anticancer drug release from mesoporous silica nanoparticles by pH-sensitive nanovalves. J. Am. Chem. Soc. **132**:12690–12697.
36. **Miceli NJ, Olson WA, Weber WW.** 1975. An improved micro spectrofluorometric assay for determining isoniazid in serum. Biochem. Med. **12**:348–355.
37. **Muttil P, et al.** 2007. Inhalable microparticles containing large payload of anti-tuberculosis drugs. Eur. J. Pharm. Sci. **32**:140–150.
38. **National Institute of Public Health P.** 2010. WHO global tuberculosis control report 2010. Summary. Cent. Eur. J. Public Health **18**:237.
39. **Pandey R, Khuller GK.** 2005. Solid lipid particle-based inhalable sustained drug delivery system against experimental tuberculosis. Tuberculosis (Edinb.) **85**:227–234.
40. **Saraogi GK, Gupta P, Gupta UD, Jain NK, Agrawal GP.** 2010. Gelatin nanocarriers as potential vectors for effective management of tuberculosis. Int. J. Pharm. **385**:143–149.
41. **Semete B, et al.** 2010. In vivo evaluation of the biodistribution and safety of PLGA nanoparticles as drug delivery systems. Nanomedicine **6**:662–671.
42. **Semete B, et al.** 2010. In vivo uptake and acute immune response to orally administered chitosan and PEG coated PLGA nanoparticles. Toxicol. Appl. Pharmacol. **249**:158–165.
43. **Sharma A, Sharma S, Khuller GK.** 2004. Lectin-functionalized poly (lactide-co-glycolide) nanoparticles as oral/aerosolized antitubercular drug carriers for treatment of tuberculosis. J. Antimicrob. Chemother. **54**:761–766.
44. **Sosnik A, Carcaboso AM, Glisoni RJ, Moretton MA, Chiappetta DA.** 2010. New old challenges in tuberculosis: potentially effective nanotechnologies in drug delivery. Adv. Drug Deliv. Rev. **62**:547–559.
45. **Souris JS, et al.** 2010. Surface charge-mediated rapid hepatobiliary excretion of mesoporous silica nanoparticles. Biomaterials **31**:5564–5574.
46. **van Hest R, et al.** 2004. Hepatotoxicity of rifampin-pyrazinamide and isoniazid preventive therapy and tuberculosis treatment. Clin. Infect. Dis. **39**:488–496.
47. **Vivero-Escoto JL, Slowing II, Trewyn BG, Lin VS.** 2010. Mesoporous silica nanoparticles for intracellular controlled drug delivery. Small **6**:1952–1967.
48. **Xia T, et al.** 2009. Polyethyleneimine coating enhances the cellular uptake of mesoporous silica nanoparticles and allows safe delivery of siRNA and DNA constructs. ACS Nano **3**:3273–3286.
49. **Xue M, et al.** 2011. pH-operated mechanized porous silicon nanoparticles. J. Am. Chem. Soc. **133**:8798–8801.
50. **Zhao Y, Vivero-Escoto JL, Slowing II, Trewyn BG, Lin VS.** 2010. Capped mesoporous silica nanoparticles as stimuli-responsive controlled release systems for intracellular drug/gene delivery. Expert Opin. Drug Deliv. **7**:1013–1029.